Extended Data for

Probing Berry phase effect in topological surface states

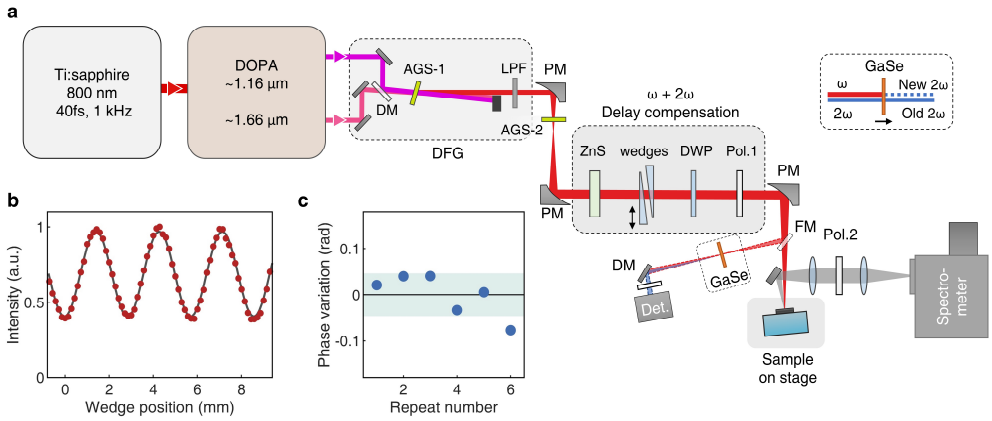

Extended Data Fig. 1 | Optical layout for the two-colour HHG measurement. a, A titanium sapphire amplifier is adopted to pump the DOPA, and after that MIR pulses are produced from near-colinear difference-frequency generation (DFG) setup then filtered by a long-pass filter (LPF). The SH beam is generated from the $AgGaS_2$ (AGS) crystal. The two-colour pulse is finally delivered into the HH measurement device after passing through an in-line phase compensator and a parabolic mirror (PM). The phase compensator composes of a ZnS plate, a pair of wedges, a dual-wavelength waveplate (DWP) and a polarizer (Pol. 1). Inset: SH interference technique for relative phase delay measurement after a flip mirror (FM), including a GaSe crystal, a dichroic mirror (DM) and a pyroelectric Detector (Det.). **b**,**c**, Oscillation curve of SH intensity recorded by adjusting relative delay (**b**), with the relative phase variation obtained by fitting the curves from successive interference measurements (**c**). The standard deviation of 0.05 radian reveals rather good phase stability of the two-colour fields.

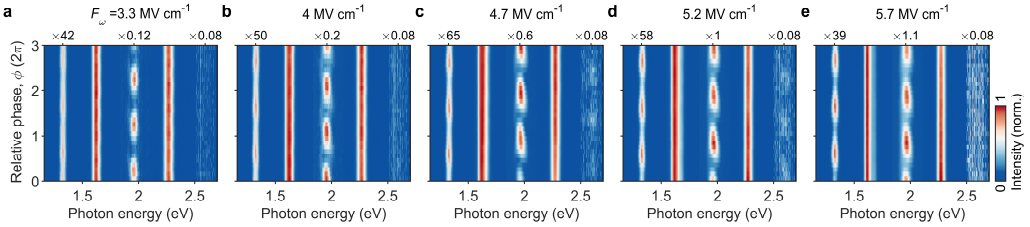

Extended Data Fig. 2 | MIR field dependence of HH spectral interferogram. High-harmonic spectrum from BSTS at an angle of 0° (pump field along $\bar{\Gamma} - \bar{\mathrm{M}}$ direction) as the function of relative phase, measured at increasing driven field strength from 3.3 to 5.7 MV cm^{-1}. Each harmonic is normalized individually, with the relative strength of which is labeled on the top. The modulation period of $T_{2\omega}$ still dominates in series of interference images, with the order-dependent modulation phase display only slightly changing.

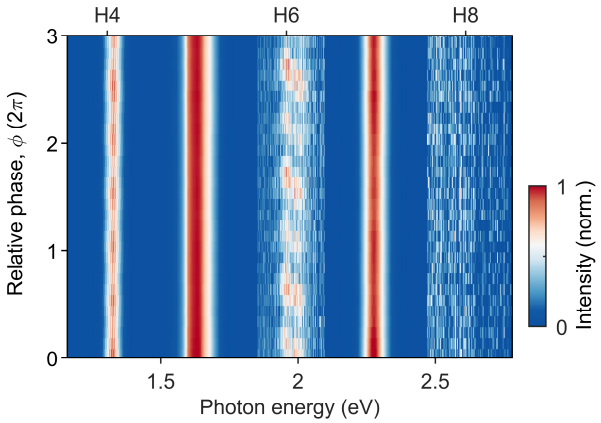

Extended Data Fig. 3 | Harmonic spectral interference pattern from BSTS at angle of 30°. Normalized high-harmonic spectrum from BSTS driven by two-colour field consisting of F_ω = 5.2 MV cm^{-1} and $F_{2\omega}$ = 120 kV cm^{-1} with polarization along $\bar{\Gamma} - \bar{\mathrm{K}}$ direction. Geometric phase effect is minimized for this crystal orientation.

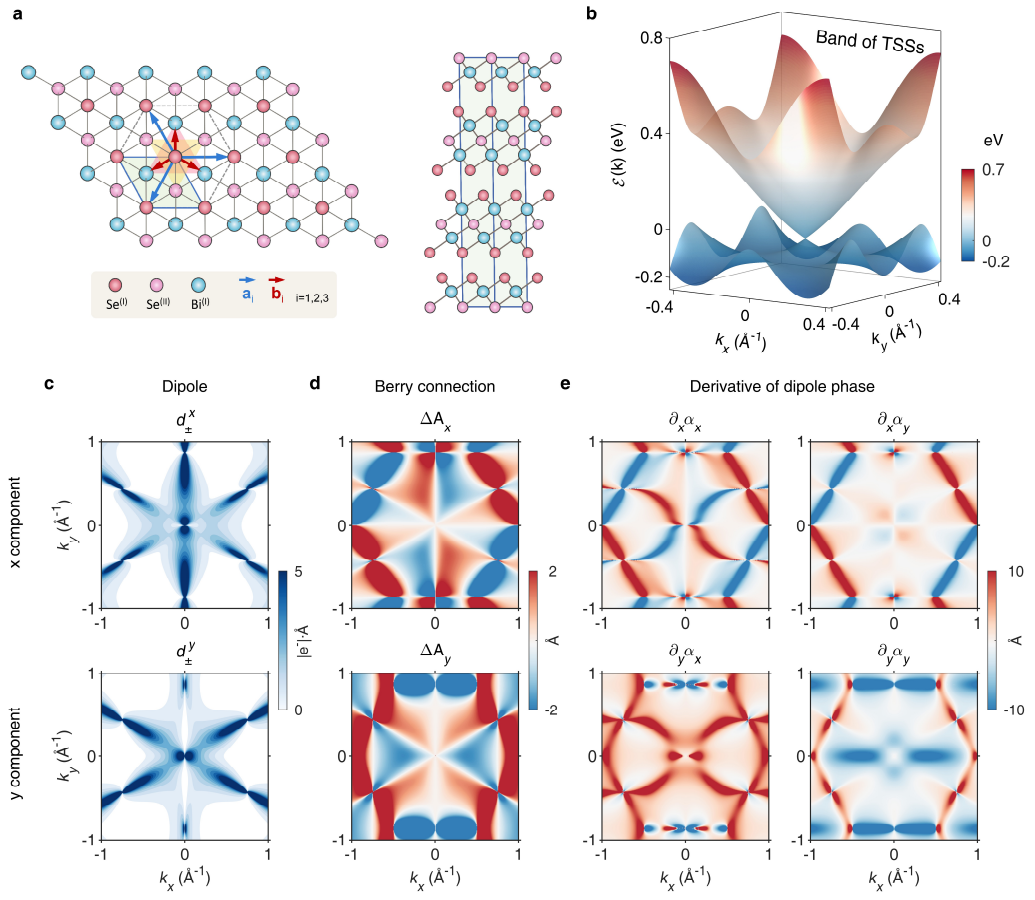

Extended Data Fig. 4 | Crystal and electronic structures of Bi_2Se_3. **a**, Tetradymite-type structure of prototypical 3D TI Bi_2Se_3. Top view (left) and side view (right) of the rhombohedral crystal structure. Five atomic layers stacked in orders $Se^{(I)}$-Bi-$Se^{(II)}$-Bi-$Se^{(I)}$ form a quintuple layer. Nearest neighbor vectors of intra-hexagonal atomic layer $\vec{a}_i$ and nearest neighbor vectors interlayers $\vec{b}_i$. **b**, Energy dispersion of the surface states obtained from the tight-band Hamiltonian. **c-e**, Transition dipole moment (**c**), difference of the Berry connections (**d**) and derivative of dipole phase (**e**) in 2D momentum space. Upper and lower horizontal rows displayed the *x* and *y* components, respectively.

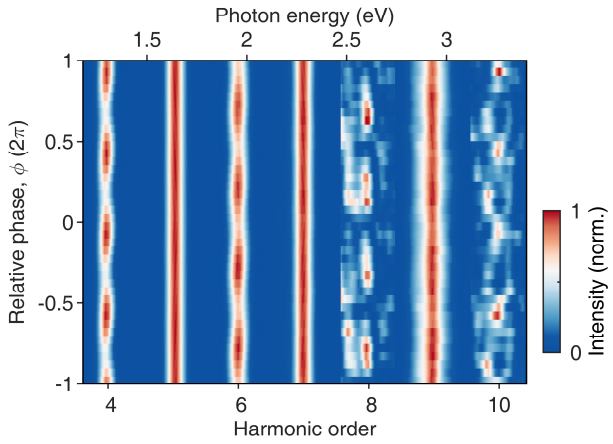

Extended Data Fig. 5 | Harmonic spectral interference pattern in the absence of geometric phase effect. In SBE computation the laser parameter and crystal orientation are the same as that of Fig. 2b in the main text, except that the Berry connection and derivative of dipole phase is artificially set to zero. The interferogram reveals the HH response in trivial energy band with qusi-relativistic dispersion.

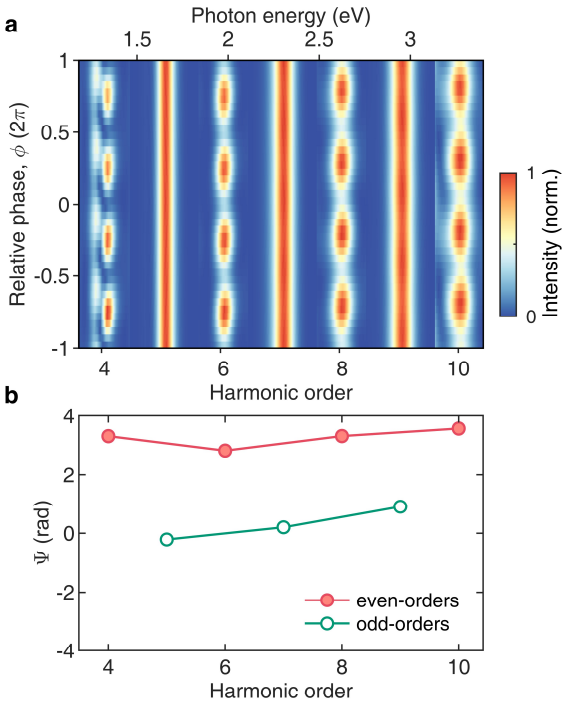

Extended Data Fig. 6 | Harmonic spectral interference pattern of bulk states. a, Simulated HH spectra from light field driven bulk electron dynamics as the function of two-colour delay at pump field strength of F_{ω} = 5.5 MV cm^{-1} and $F_{2\omega}$ = 120 kV cm^{-1}. **b**, Phases of $T_{2\omega}/2$ modulation extracted from the intensity oscillation curve. The broken lines are a guide to the eye. The optimal phases show weak dependence on the harmonic order.

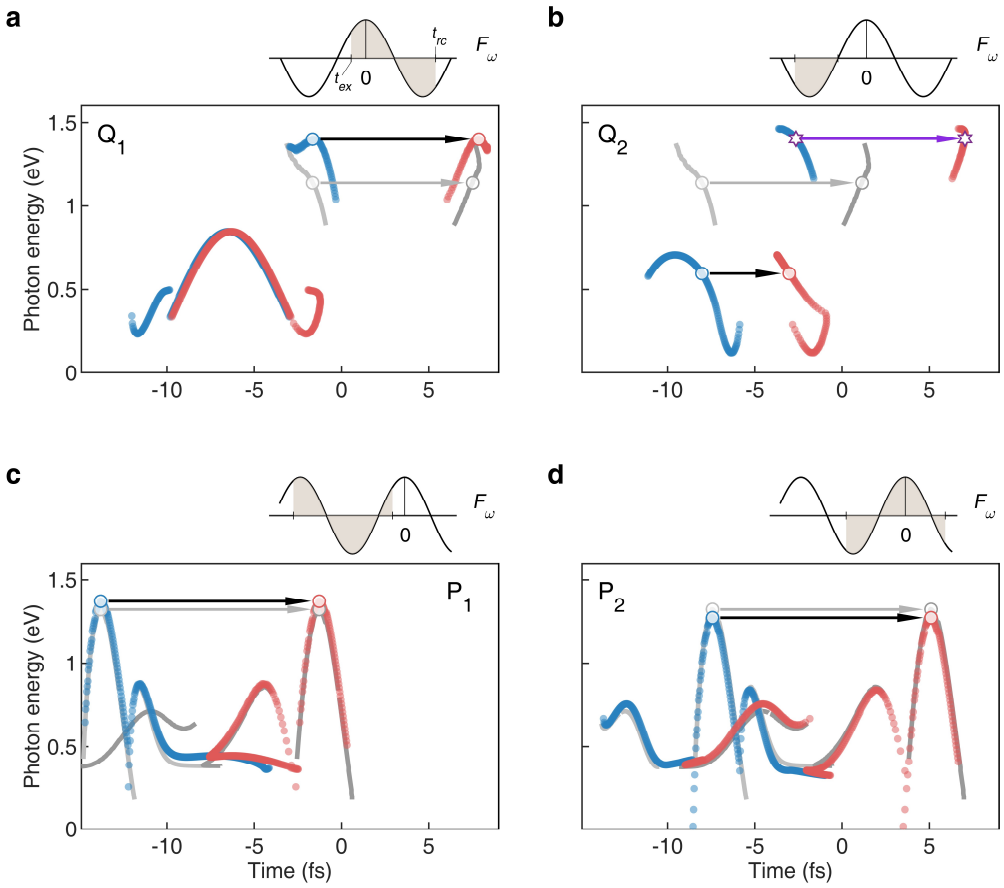

Extended Data Fig. 7 | Semiclassical image of time-frequency HH emission. a-d, Classical orbits for *e-h* pairs initiated from four ***k*** points, Q_1 (**a**), Q_2 (**b**), P_1 (**c**), P_1 (**d**), of interest are plotted separately. Harmonic photon energy as the function of excitation time (blue dots) and recollision time (red dots) is obtained by solving the saddle point conditions with the action of geometric phase factor. In parallel, time-frequency profiles by neglecting the geometric phase effect are also plotted (gray curves). The arrows connecting the white dots represent the time of evolution and resultant photon energy from the recollision paths as shown in Fig. 4d,e of the main text. The purple arrow and hexagrams illustrate the recollision event reshaped by the remarkable Berry phase effect. Insets: The fundamental waveform (black line) and the variation of vector potential between the birth and recombination times (area of grey shaded region).

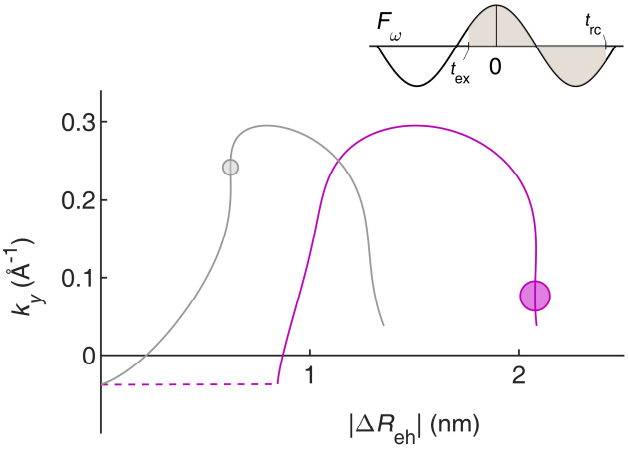

Extended Data Fig. 8 | Berry phase effect boosts harmonic photon energy. Semiclassical trajectory initiate from Q_2 excited at t_{ex} = −0.6 fs (purple curve) in parametric space, corresponding to the purple arrow and hexagrams in Extended Data Fig. 7b. Trajectory in the removal of geometric phase effect is plotted in grey curve. Recollision path is markedly reshaped by the Berry phase effect, resulting in a significant enhancement of recollision energy. Inset: The fundamental waveform (black curve) and the variation of vector potential between the birth and recombination times (area of grey shaded region).